(Received 27 September 2023, Accepted 5 December 2023, Scheduled 19 December 2023)

Design of Spatial Magnetic Field Measurement System and Experimental Study of Near-Field Characteristics in Wireless Power Transfer System

Deyu Zeng, Jianwei Kang*, Xiangyang Shi, and Yang Shi

Key Laboratory of Testing Technology for Manufacturing Process, Ministry of Education
Southwest University of Science and Technology, Mianyang 621010, China

ABSTRACT: Magnetic coupling resonant wireless power transfer (WPT) technology is widely used in a lot of power equipment because of its high efficiency and safety. Magnetic field is a key factor to study the energy transmission mechanism and transmission characteristics of WPT system. At present, the research on the WPT system spatial magnetic field mainly focuses on theoretical research and finite element simulation, with relatively little experimental research. This paper aims to establish an experimental platform for a WPT system, propose and design a magnetic field measurement system suitable for the WPT system, and conduct experimental research on the WPT system magnetic field with the measurement system. The near field region of the magnetic field is divided, and the experimental magnetic field distribution law is obtained using dimensionless and surface fitting methods. Finally, different models are obtained by surface fitting to characterize the distribution law of the experimental magnetic field. The results indicate that the dimensionless magnetic field intensity follows different forms of exponential distribution in different regions. The models are in good agreement with the actual distribution of the magnetic field, which can effectively reflect the variations in actual magnetic field intensity.

1. INTRODUCTION

Magnetic coupling resonant wireless power transfer (MCR-WPT) technology has higher energy transmission efficiency, higher security, and longer transmission distance than inductive power transfer [1]. It has become a research hotspot in WPT. WPT technology makes electronic equipment more flexible to be used in some special occasions, such as implantable medical equipment [2, 3] and underwater equipment [4–6]. WPT technology also effectively avoids the problem of line aging, loss increases, etc.

Magnetic field, as the medium [7] of energy transmission in magnetic coupling resonant WPT system, is closely related to the energy transmission efficiency [8, 9] and the power of WPT system. When the system is working, stray magnetic [10, 11] field will be generated in the nearby space. Besides, the harmonic current generated by the system detuning and its own high-frequency switching circuit will increase the generation [12] of leakage magnetic field. The magnetic field will have an impact on other electronic components and living organisms [13] around the system. For that reason, in terms of the electromagnetic shielding [14], electromagnetic compatibility, and safety [15] of WPT systems, it is necessary to study the distribution characteristics and variation rules of magnetic field of WPT systems in actual working conditions.

In many literatures, the research on magnetic field of WPT system is mainly through the theory and simulation. Ref. [16] studied the theoretical formula of the magnetic field intensity of a planar spiral coil and gave the distribution maps of the horizontal and vertical components of the magnetic field intensity on the horizontal plane at different distances from the coil plane. Refs. [17, 18] carried out theoretical research on the magnetic field distribution in the space around the single-turn circular coil and gave the expression of the magnetic field intensity in the space through Biot-Savart law. Among them, [17] gave the three-dimensional distribution diagram of the magnetic field, as well as the distribution diagram of the incident and reflected magnetic field on the coil plane, using finite element simulation. Ref. [18] put forward the optimization algorithm of the magnetic field calculation and gave the three-dimensional magnetic field intensity distribution diagram under different discrete precisions. Ref. [19] carried out theoretical research on an n-turn cylindrical spiral coil and obtained the magnetic flux density by calculating the electric field intensity, but did not give the distribution of the magnetic field intensity of the coil in space. In [20, 21], the magnetic field distributions of planar rectangular and spiral coils were obtained by finite element simulation. However, the coil model is simplified in the simulation, ignoring the details and complexity of the actual system. In the theoretical analysis of the magnetic field, the numerical calculation method may introduce and accumulate errors, so the two research methods are difficult to present the actual distribution of the system magnetic field. Above all, there are few experimental studies on the magnetic field distribution of WPT system. Most literature verifies the correctness of the theoretical or simulation results by calculating the energy transmission efficiency of the actual system.

* Corresponding author: Jianwei Kang (kjw689@163.com).

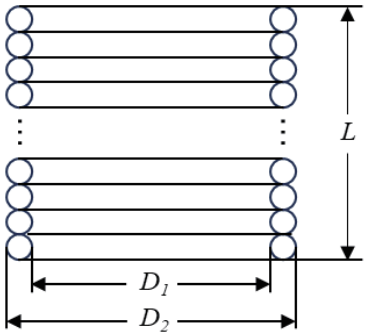

FIGURE 1. Schematic diagram of the cross-section of induction coil.

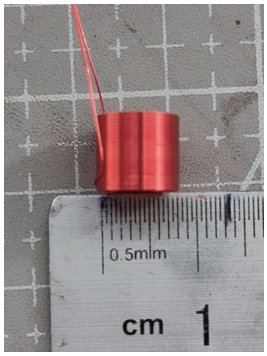

FIGURE 2. Magnetic field probe.

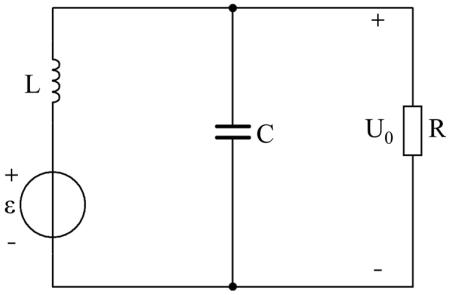

FIGURE 3. Measuring circuit equivalent circuit.

Therefore, this paper studies the actual distribution characteristics of the spatial magnetic field in the WPT system from an experimental perspective. We constructed a WPT system, designed a magnetic field measurement system for the WPT system we are studying, and measured the spatial magnetic field of the WPT system to study the distribution characteristics. In the experimental study of the WPT system spatial magnetic field, the magnetic field measurement system was used to measure the magnetic field intensity of the space points. The distribution of the output voltage of the magnetic field measurement system was obtained. Based on the distribution characteristics of the voltage, two characteristic voltages were defined. Then the experimental data were dimensionless processed, and the dimensionless voltages and dimensionless parameters were determined. Finally, the magnetic field distribution law was obtained by fitting the two-dimensional surface. The results show that the spatial magnetic field of the system is subject to different forms of exponential distribution, which provides a certain foundation and support for electromagnetic safety and other problems in the near space.

2. DESIGN AND RESEARCH OF MAGNETIC FIELD MEASUREMENT OF WPT SYSTEM

2.1. Theoretical Basis of the Magnetic Field Probe

Magnetic field measurement methods are many, such as Hall effect method, magneto-optical effect method, fluxgate method, magnetoresistive effect method, and electromagnetic induction method. We combine with the existing laboratory conditions and the characteristics of the magnetic field to be measured, and the electromagnetic induction method was chosen to measure the spatial magnetic field of the WPT system.

The electromagnetic induction method is a simple and practical method to measure the alternating magnetic field, and its basic principle is Faraday's electromagnetic induction law. The mathematical expression of the law is:

$$\varepsilon = -\frac{d\phi}{dt} = -\frac{d\left(\oint_s \mathbf{B}\cdot d\mathbf{S}\right)}{dt} \tag{1}$$

For the WPT system studied, its spatial magnetic field is symmetric about the central axis. Thus, the radial and axial components of the WPT system spatial magnetic field need to be measured respectively to calculate the synthetic magnetic field.

From the above formula, the output voltage of the measuring circuit is directly proportional to the magnetic field intensity. Therefore, the output voltage of the measuring circuit can be used to represent the magnetic field intensity. Then the synthetic magnetic field intensity can be expressed by the following formula.

$$B = (B_r + B_z)^2 \propto (U_r + U_z)^2 \tag{2}$$

where U_r, U_z, B_r, and B_z represent radial and axial components of the output voltage and magnetic field, respectively.

2.2. Design of Magnetic Field Probe

The magnetic field probe uses a single thin wall induction coil. Because the coil is used to measure the magnetic field intensity of the space point, and the coil has a certain volume, which leads to the uncertainty of the measured space point, the size of the coil needs to be reduced. However, one hopes to increase the size of the coil to improve the obtained amplitude of the signal on the coil, so the size of the coil needs to be optimized. The section of the thin wall induction coil is shown in Figure 1, where D_1 is the outer diameter of the coil, D_2 the inner diameter of the coil, and L the length of the coil.

When the coil geometry meets $L/D \approx 0.866$ for a single thin wall coil, one can approximate that the measurement result by the coil is the magnetic field intensity at the central space point of the coil. Meanwhile, since the magnetic field intensity of the space point needs to be measured, the size of the magnetic field probe needs to be as small as possible. However, a smaller probe will generate a smaller signal which may not be measured. The magnetic field intensity is $10^{-6} \sim 10^{-4}$ T, so the probe size should be considered comprehensively. The main parameters of the probe are shown in Table 1.

The actual probe is shown in Figure 2.

TABLE 1. Parameters of the probe.

Parameter	Value
Internal diameter	8 mm
Wire diameter	0.21 mm
Number of turns	33

2.3. Signal Processing Circuit Design in Magnetic Field Measurement System

The induced electromotive force is proportional to the frequency of the magnetic field, according to the law of electromagnetic induction. To reduce the impact of frequency fluctuations, an integration circuit is incorporated into the measurement circuit.

This circuit will achieve a linear relationship between the voltage of the measurement circuit and the magnitude of the magnetic field, while the voltage is independent of the frequency of the magnetic field. The equivalent circuit of the induction coil with the integration circuit is shown in Figure 3.

In Figure 3, ε represents the induced electromotive force; L and R represent the induction coil of the magnetic field probe and its internal resistance respectively; C represents the integrated capacitance; and R_L represents the integrated matching resistance. After adding the integral link, the relationship between magnetic field intensity and voltage can be expressed based on the Faraday's law and Kirchhoff's voltage law (KVL):

$$-NA\frac{dB}{dt} = LC\frac{dU_0^2}{dt^2} + \frac{L}{R}\frac{dU_0}{dt} + U_0 \tag{3}$$

The transfer function can be shown further after applying Laplace transform and considering $s = j\omega$:

$$T = NA\frac{j\omega}{1 - LC\omega^2 + j\dfrac{L}{R}\omega} \tag{4}$$

Combining $\omega_0 L = 1/\omega_0 C = R_L/Q$, the transfer function is:

$$T = \frac{NA\omega_0}{\dfrac{1}{Q} + j\left(\dfrac{\omega}{\omega_0} - \dfrac{\omega_0}{\omega}\right)} \tag{5}$$

When the frequency of magnetic field is approximately equal to ω_0, the transfer function of the magnetic field measurement circuit is

$$T = \left|\frac{U}{B}\right| = NA\omega_0 Q, \tag{6}$$

where N is the number of coil turns, A the cross-sectional area of the coil, ω_0 the resonant frequency, and Q the quality factor of the coil.

The geometric size of the induction coil is relatively small, in order to ensure the accuracy of measurement, resulting in the induction electromotive force generated by the coil being relatively weak. So, an amplification processing is necessary. The amplifier circuit chip is AD8421, which is a high-speed instrument amplifier with low noise, and it still maintains relatively flat amplitude-frequency characteristics in the case of a high gain, especially suitable for measuring high-speed low-level signals. The AD8421 sets the gain through the jumper resistor, which is shown in Figure 4. The resistor in the circuit uses a precision resistor with 1% accuracy, in order to ensure the accuracy of amplification.

2.4. Design and Debugging of the Experimental Platform

The experimental platform was built as shown in Figure 5, in order to obtain the spatial magnetic field distribution of the magnetic coupling resonant WPT system. The experimental platform mainly includes a programmable DC power supply, an inverter circuit, a coupling mechanism, and a resonant topology circuit.

In the established magnetic coupling resonant WPT system, both the transmitting coil and receiving coil are made of a solenoid coil. The coupling mechanism, as the transmitting coil and receiving coil, adopts the same structure and parameter. The parameters are shown in Table 2.

TABLE 2. Parameters of the coupling mechanism.

Parameter	Value
Internal diameter	210 mm
Cross sectional area of wire	2.5 mm^2
Number of turns	8

The resonant topology compensation circuit adopts series-series structure, and the parameters of the topology compensation circuit are shown in Table 3.

TABLE 3. Parameters of topology compensation circuit

Parameter	Value
Current in primary side	1.28 A
Frequency	20 kHz
Compensation capacitor	2.53 μF
Load	1 Ω

The WPT system studied chooses 20 kHz as the power frequency. One significant reason is that long-distance power transmission efficiency tends to be relatively high at this frequency. Then, another reason is safety. The WPT system employed at this frequency enables efficient and safe transfer in short to medium-range distances. The WPT system at 20 kHz is mainly utilized in some fields, such as electric vehicles and implantable medical devices.

In the experiment, the current phase difference between the transmitting coil and receiving coil is approximately $89^\circ \sim 93^\circ$, which can be considered that the built system is in a resonant state. Figure 6 shows the test results of the magnetic field measurement system.

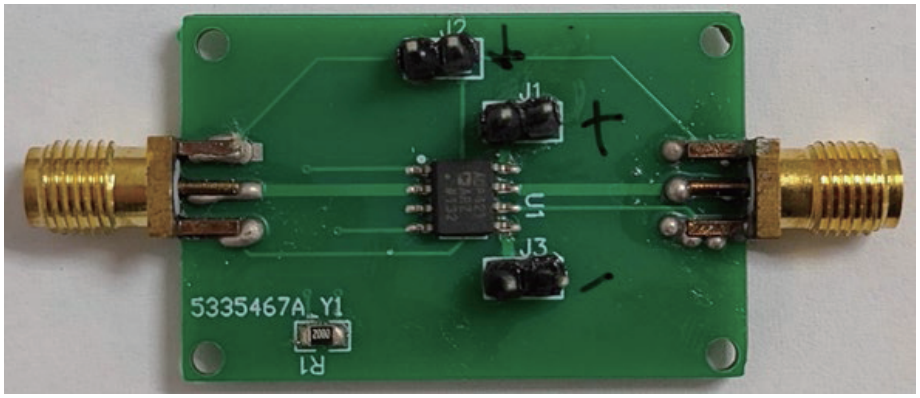

FIGURE 4. Amplifying circuit.

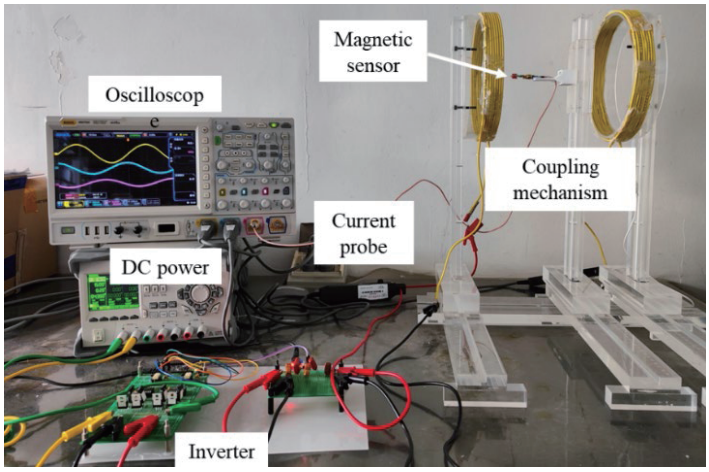

FIGURE 5. Experiment platform of WPT system.

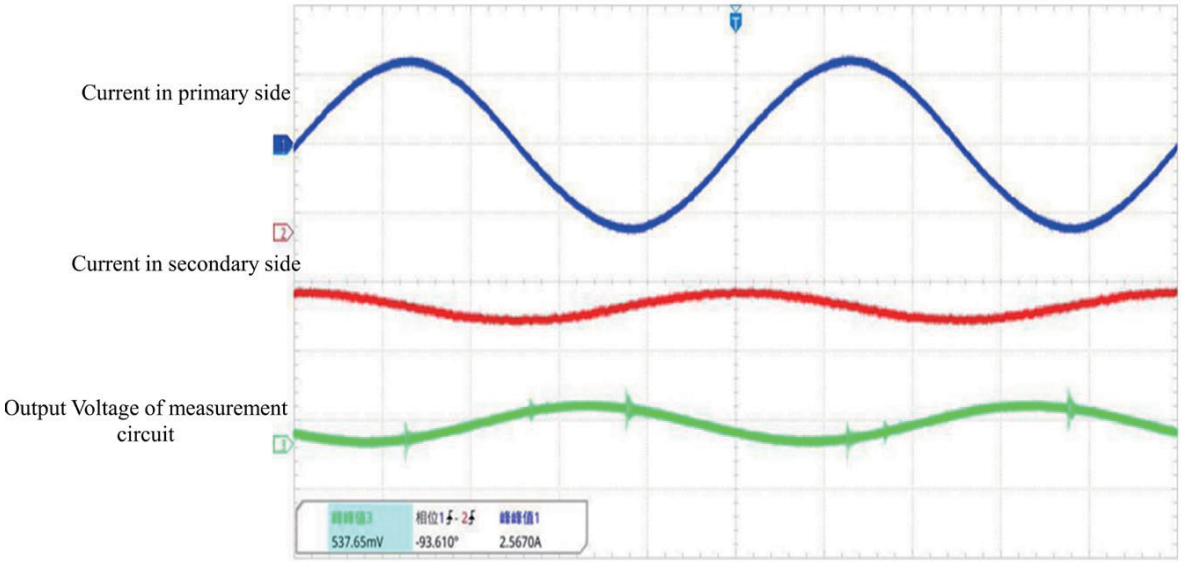

FIGURE 6. Test results of magnetic field measurement system.

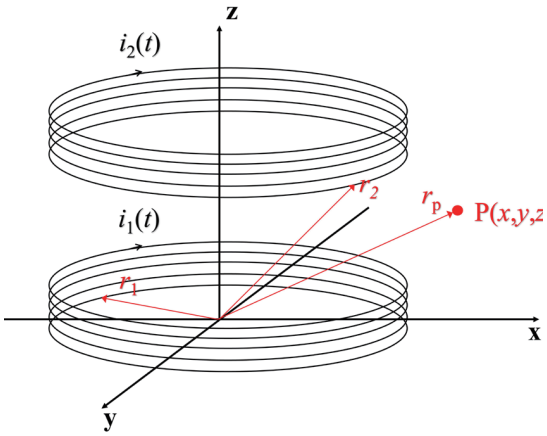

FIGURE 7. Two-coil model of the system.

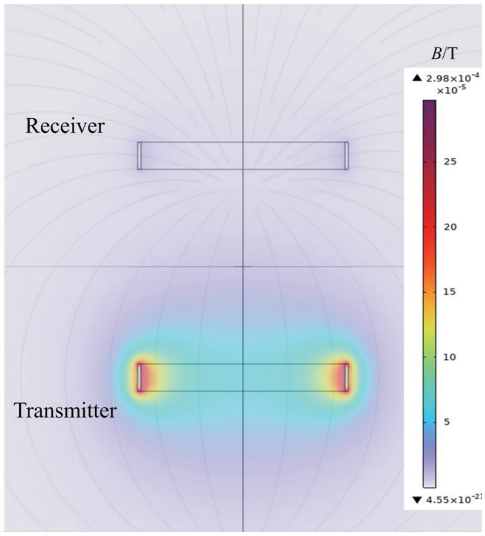

FIGURE 8. Simulation results of the system spatial magnetic field.

3. THEORETICAL RESEARCH ON SPATIAL MAGNETIC FIELD CHARACTERISTICS OF WPT SYSTEM

A calculation model of the spatial magnetic field of the system must be established first to study the spatial magnetic field characteristics of WPT system. Figure 7 shows the WPT system studied in this paper. The transmitting coil and receiving coil are parallel to each other, with the same parameters.

i_1(t) and i_2(t) indicate currents in the transmitting and receiving coils; r_1, r_2, and r_p represent the source and field position vectors on the coil, respectively.

The system coil shown in Figure 7 is symmetric about the central axis, so only the magnetic field in the xOz plane is selected as the object.

When the system enters a steady state, according to the superposition principle, the magnetic field intensity in space is composed of the magnetic fields generated by the transmitting coil and receiving coil, respectively:

$$H(x,z) = H_1(x,z) + H_2(x,z) \tag{7}$$

where subscripts 1 and 2 stand for the transmitting coil and receiving coil, respectively.

The magnetic field intensity at any point can be calculated with Biot-Savart law:

$$H(x,z) = \frac{\mu_0}{4\pi}\left(\oint_{l_1} \frac{i_1 \cdot dl_1 \times (r_1 - r_p)}{|r_1 - r_p|^3} + \int_{l_2} \frac{i_2 \cdot dl_2 \times (r_2 - r_p)}{|r_2 - r_p|^3}\right) \tag{8}$$

The distribution of the spatial magnetic field of the system on the xOz plane is obtained by a finite element simulation, as shown in Figure 8.

The theoretical results show that the closer the current source is, the stronger the magnetic field is. For solenoid coils, the simulation shows that the magnetic field is mainly concentrated in the middle of the coil.

However, in the finite element simulation, due to the simplification of the model, the results are different from the actual magnetic field. It is necessary to carry out experimental research on the magnetic field. The next section will carry out the experimental study on WPT system spatial magnetic field. Different characteristic voltages and parameters are defined for dimensionless processing.

4. EXPERIMENTAL RESEARCH ON SPATIAL MAGNETIC FIELD CHARACTERISTICS OF WPT SYSTEM

4.1. Measurement and Results

The WPT system and coordinate system are shown in Figure 9. In this section, the studied space area of the magnetic field is set as a rectangular area with a width of 156 mm and a height of 192 mm, which is the red region in Figure 9.

During measuring, the transmitting coil and receiving coil of the system remain stationary, and the center point of the induction coil of the magnetic field probe coincides with the central axis of the transmitting coil. Starting from $r = 0$ mm, $z = 8$ mm, one space point is taken every 4 mm along the axial and radial directions of the coordinate system. In addition, since the wire diameter of the transmitting coil wire is 3.5 mm, the torus of $r = 106$ mm is approximately the middle torus of the coil wire. From the space $r = 106$ mm, $z = 8$ mm, 47 points are selected and measured in the direction of the z axis. A total of 1927 space points were selected in this way. At the set points, the radial component and the axis component of the magnetic field intensity are measured by the above measuring system.

The output voltage of the measuring system representing the radial and axial components of the spatial magnetic field is obtained, and the voltage used to represent the synthetic magnetic field intensity is calculated. The voltage distribution is plotted in the graph with the radial distance as the X axis, the axial

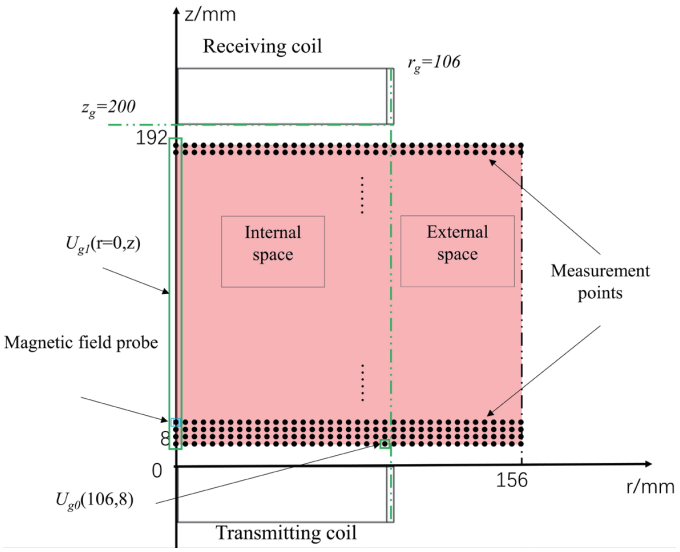

FIGURE 9. Schematic diagram of the WPT system and the coordinate system.

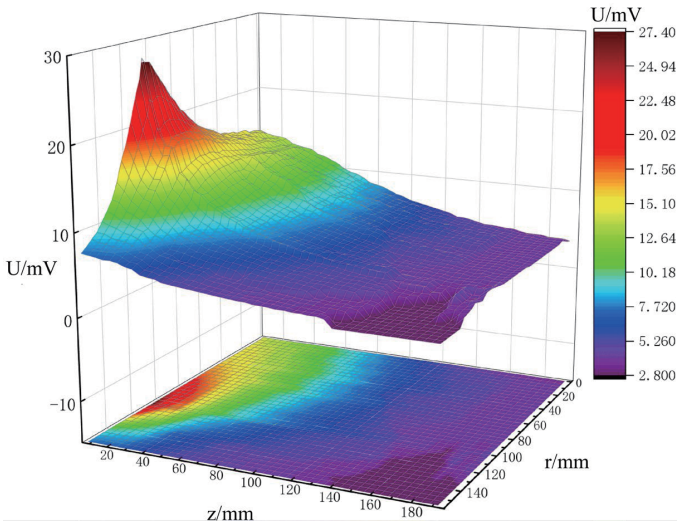

FIGURE 10. Voltage distribution surface.

distance as the Y axis, and the amplitude as the Z axis. The voltage distribution surface is obtained as shown in Figure 10.

The magnetic field intensity near the transmitting coil is generally larger than that in other regions, as shown in Figure 10. At the same time, the closer the distance is from the transmitting coil, the more drastic the variation of the magnetic field intensity is. In the axial direction, the magnetic field shows monotonically decreasing, and the decay rate is inconsistent in different regions. In the radial direction, the magnetic field intensity increases and then decreases near the transmitting coil. Differently, the magnetic field shows monotonically decreasing away from the transmitting coil. Overall, the variation trend of the voltage distribution surface is basically consistent with the simulation results.

4.2. Dimensionless Characteristic Geometric Parameters and Characteristic Voltage

The synthetic magnetic field of the WPT system can be represented by the output voltage of the measurement system, according to the above measurement principle. We will use the voltage to analyze the magnetic field. The near field of the WPT magnetic field will be divided, and a characteristic of the magnetic field from experiment will be obtained. The following section represents the work of the data processing procedure.

First of all, the deviation of the discrete distribution surface of the output voltage of the measuring circuit at a certain point in the r-z plane is defined as:

$$\begin{cases} T_r(r,z) = \dfrac{\partial U_r(r,z)}{\partial r} = U_r(r+1,z) - U_r(r,z) \\ T_z(r,z) = \dfrac{\partial U_z(r,z)}{\partial z} = U_z(r,z+1) - U_r(r,z) \end{cases} \tag{9}$$

where $T_r\,(r,z)$ and $T_r\,(r,z)$ respectively represent the radial difference and axial difference of the measured system output voltage at the spatial coordinates. The deviation represents the degree of rapid variation of magnetic field intensity in space, enabling the magnetic field distribution surface to exhibit mathematical characteristics.

Then, the characteristic parameters are precisely defined, according to the voltage differentiation result. The distributions of radial difference and axial difference of the voltages on the r-z plane in the study area, shown in Figure 11 and Figure 12, are obtained from Equation (7). The transmitting coil with a radius of 105 mm and a wire section diameter of 3.5 mm is equivalent to a thin-walled ring with a radius of 106 mm.

The results above indicate that the voltage variations are the sharpest in the region near the transmitting coil. Combined with Figure 10, Figure 11, and Figure 12, the synthetic magnetic field intensity has a maximum value point in the region near the transmitting coil.

The distribution and variation of the magnetic field are inconsistent at different positions. To obtain the accurate fitting model in the next section, it is necessary to partition the spatial magnetic field. The WPT system space is divided into inner and outer regions with the radius of 106 mm as the boundary. In the different regions, the characteristic parameters are found to be used in the fitting processing.

The magnetic field generated by the WPT system in space reaches its maximum value at $r = 106$ mm and $z = 8$ mm in the area, and the output voltage $U(r = 106, z = 8)$ at this point is defined as the characteristic voltage U_{g0}. In the inner region of the system, the output voltage $U(r = 0, 8 \le z \le 192)$ on the central axis of the transmitting coil can be approximately considered as the minimum value, so it is defined as the characteristic voltage U_{g1}.

At the same time, the distribution characteristic of the system magnetic field depends on the geometry of the transmitting coil and receiving coil, according to theoretical Equation (5). The inner diameter of the ring is defined as the characteristic radial

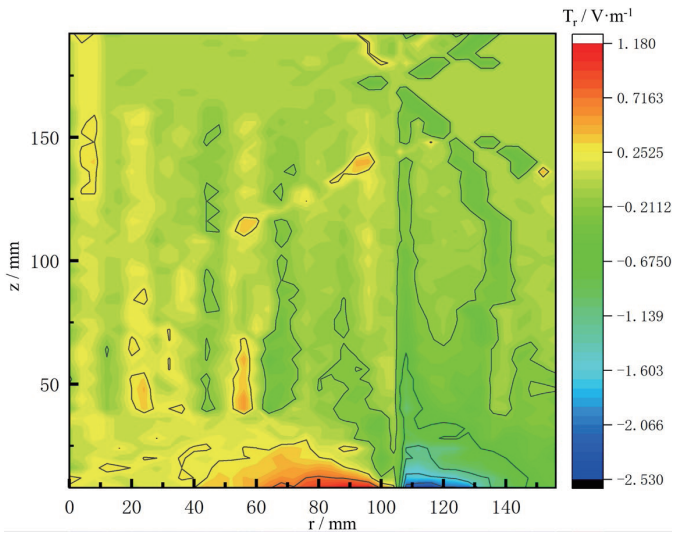

FIGURE 11. Distribution of the T_r.

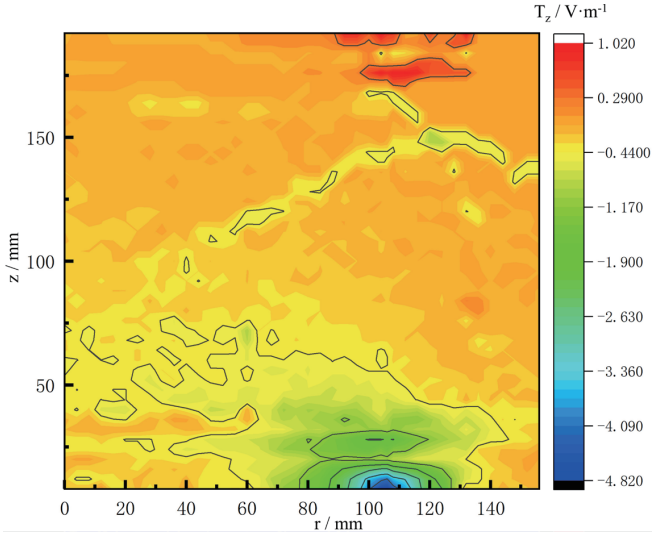

FIGURE 12. Distribution of the T_z.

distance r_g in combination with Figure 11 and Figure 12. In addition, the distance between the transmitting coil and receiving coil of the WPT system is defined as the characteristic height z_g.

5. WPT SYSTEM SPACE VOLTAGE AND SURFACE FITTING

The characteristic voltage and parameters have been defined in different regions. In this section, different models are determined with surface fitting, which are more concise than the theoretical equation. Besides, the models reflect the variations in actual magnetic field intensity and describe the distribution law as realistic as possible. Before the surface fitting, dimensionless processing is one key process. It is necessary to use the dimensionless method to eliminate the dimensional differences between variables and retain the correlation between variables, to ensure the accuracy of the subsequent two-dimensional surface fitting models.

5.1. Dimensionless And Surface Fitting of the Voltage in the System Internal Space

Within the scope of the internal space of the system, i.e., $r < 106$ mm, one defines the new dimensionless radial distance r_1^+, height z_1^+, and voltage U_1^+.

$$\begin{cases} r_1^+ = \dfrac{r_g - r}{r_g} \\ z_1^+ = \dfrac{z}{z_g} \\ U_1^+ = \dfrac{U - U_{g1}}{U_{g0}} \end{cases} \tag{10}$$

The distribution characteristic of the dimensionless voltage measured in this experiment is shown in Figure 13.

According to the above dimensionless processing, the surface fitting relationship between voltage and radial distance and height can be calculated:

$$U_1^+(r,z) = \frac{-d_1}{1 + \exp\left(\dfrac{(r/a_1)^2 + (z/b_1)^2}{c_1}\right)} \tag{11}$$

where a_1, b_1, c_1, and d_1 are constants, $a_1 = 0.432$, $b_1 = 1.304$, $c_1 = 0.007$, $d_1 = -0.711$.

5.2. Dimensionless and Surface Fitting of the Voltage in the System External Space

Within the scope of the outer space of the system, i.e., $106\,\text{mm} < r \leq 156\,\text{mm}$, one defines the new dimensionless radial distance r_2^+, height z_2^+ and voltage U_2^+.

$$\begin{cases} r_2^+ = 1 - \dfrac{r - r_g}{r_g} \\ z_2^+ = \dfrac{z_g - z}{z_g} \\ U_2^+ = \dfrac{U}{2U_{g0}} \end{cases} \tag{12}$$

The distribution law of the dimensionless voltage U_2^+ measured in this experiment is shown in Figure 14.

Similarly, the surface fitting relationship between voltage and radial distance and height is calculated:

$$U_2^+(r,z) = a_2 * \exp((r+b_2)^2 + (z+c_2)^2) + d_2 \tag{13}$$

where a_2, b_2, c_2, and d_2 are constants, $a_2 = 9.939 * 10^{-5}$, $b_2 = 1.097$, $c_2 = 1.425$, $d_2 = 0.056$.

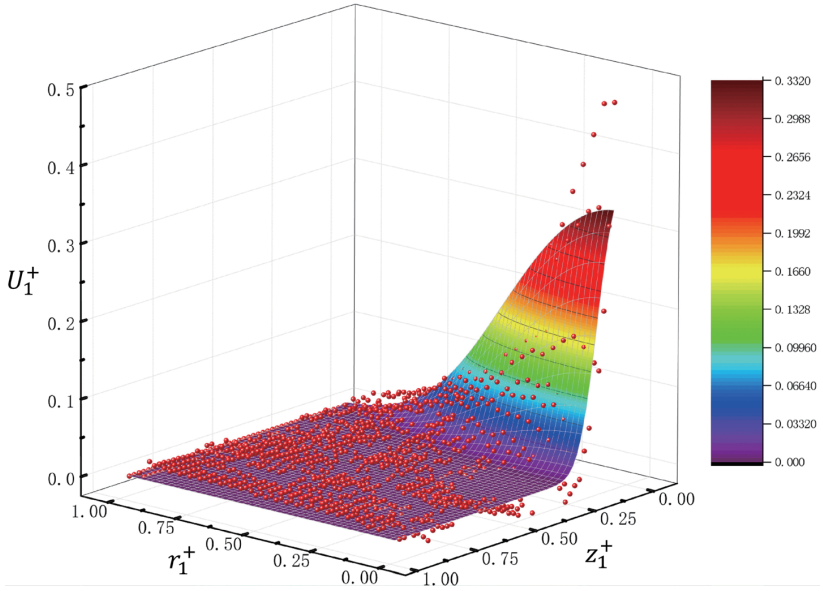

FIGURE 13. The distribution of dimensionless voltage U_1^+ in r-z plane.

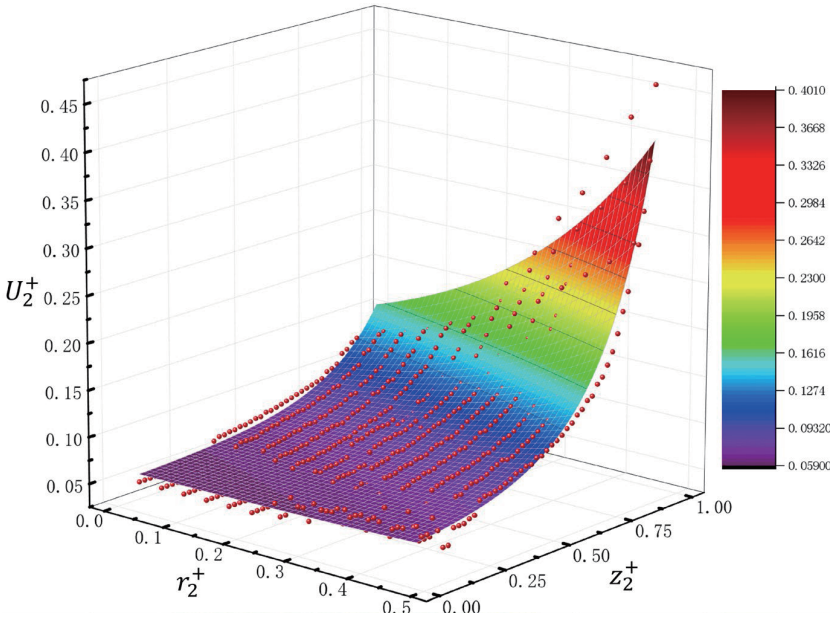

FIGURE 14. The distribution of dimensionless voltage in U_2^+ r-z plane.

5.3. Discussion of Magnetic Field Intensity Distribution Law of WPT System

The magnetic field intensity distribution law of WPT system in space can be summarized as follows:

$$\begin{cases} U_1^+ = \dfrac{-d_1}{1+\exp\left(\dfrac{(r/a_1)^2+(z/b_1)^2}{c_1}\right)} \\ U_2^+ = a_2 * \exp((r+b_2)^2+(z+c_2)^2)+d_2 \end{cases} \tag{14}$$

From the above fitting results, in the region close to the coil, the closer the coil is, the higher the magnetic field intensity is. In the region farther away from the coil, the magnetic field intensity decreases rapidly and tends to be flat. At the same time, the variation trend of the magnetic field is sharp in the region with high magnetic field intensity. In the area of low magnetic field intensity, the trend of magnetic field variation is gentle. In general, it is observed that the fitting effect is poor in the area near the coil, and the error is significantly larger than that in other areas, which is the main source of fitting error. However, in other regions, the fitting errors of the surface and the actual data are small, and the accuracy of the fitting results is still reliable.

From the experimental research, the models obtained by fitting are more concise than the theoretical analytical calculation.

The proposed models can effectively reduce the complexity of theoretical analysis and provide a certain help for the electromagnetic safety of WPT system caused by leakage magnetic field in the near space.

6. CONCLUSION

In this paper, the magnetic field probe and its signal processing circuit are designed and used in the experimental study of WPT system spatial magnetic field. The output voltage discrete distribution surface of the measuring system is obtained through experiments to characterize the spatial magnetic field of the WPT system. The dimensionless processing of system parameters and voltage is carried out, and the distribution characteristics of the spatial magnetic field of the system are studied by surface fitting. The experimental formulas for calculating the magnetic field intensity are obtained.

Firstly, a small size magnetic field probe and its signal processing circuit are designed for a two-coil WPT system, including the design of magnetic field probe and the signal processing circuit. Secondly, the experimental platform of WPT system is built, and the magnetic field of the system is measured by the designed magnetic field measurement system. The discrete distribution surface of the measurement system output voltage is obtained. The system space is divided into two regions, according to the characteristics of the system parameters and voltage distribution. In the respective region, the characteristic geometric parameters and voltages are defined and used in the dimensionless processing of the system parameters and voltage. Finally, different models are determined by carrying out surface fitting, with obtaining the distribution characteristics of the magnetic field in different regions. In general, the error of the model mainly comes from the area where the magnetic field intensity changes sharply, that is, near the transmitting coil. However, in other locations of the study area, the models are in good agreement with the actual distribution of the magnetic field. The models effectively describe the distribution characteristics and variations of the magnetic field in the whole space of the WPT system. The distribution law reflected by the models is reasonable. The models can simplify the analysis of spatial magnetic field in WPT system.

In this paper, only the magnetic field between the two coils of the WPT system was studied. In the subsequent research, the distribution characteristics of the magnetic field in the adjacent space outside the system can be continued to be paid attention to. Studying the magnetic field in this area has certain practical significance for the follow-up research on the electromagnetic compatibility of the WPT system in engineering applications.

ACKNOWLEDGEMENT

This work was supported financially by the National Natural Science Foundation of China (Grant No. 52007159), and the Natural Science Foundation of Southwest University of Science and Technology (Grant No. 20zx7116).

REFERENCES

[1] Chen, Z., X. Sun, B. Ren, Z. Wang, and J. Liu, "Analysis of four-coil magnetic resonance coupling wireless power transfer system based on LCC-SSS compensation network," *Energy Reports*, Vol. 9, No. 3, 419–427, May 2023.

[2] Barbruni, G. L., P. M. Ros, D. Demarchi, S. Carrara, and D. Ghezzi, "Miniaturised wireless power transfer systems for neurostimulation: A review," *IEEE Transactions on Biomedical Circuits and Systems*, Vol. 14, No. 6, 1160–1178, Dec. 2020.

[3] Khan, S. R., S. K. Pavuluri, G. Cummins, and M. P. Y. Desmulliez, "Wireless power transfer techniques for implantable medical devices: A review," *Sensors*, Vol. 20, No. 12, Jun. 2020.

[4] Mohsan, S. A. H., A. Islam, M. A. Khan, A. Mahmood, L. S. Rokia, A. Mazinani, and H. Amjad, "A review on research challenges, limitations and practical solutions for underwater wireless power transfer," *International Journal of Advanced Computer Science and Applications*, Vol. 11, No. 8, 554–562, Aug. 2020.

[5] Kim, J., K. Kim, H. Kim, D. Kim, J. Park, and S. Ahn, "An efficient modeling for underwater wireless power transfer using z-parameters," *IEEE Transactions on Electromagnetic Compatibility*, Vol. 61, No. 6, 2, SI, 2006–2014, Dec. 2019.

[6] Xu, F. and H. Huang, "Frequency selection for underwater wireless power transfer based on the analysis of eddy current loss," *AEU-International Journal of Electronics and Communications*, Vol. 163, May 2023.

[7] Wei, X., Z. Wang, and H. Dai, "A critical review of wireless power transfer via strongly coupled magnetic resonances," *Energies*, Vol. 7, No. 7, 4316–4341, Jul. 2014.

[8] Kurs, A., A. Karalis, R. Moffatt, J. D. Joannopoulos, P. Fisher, and M. Soljacic, "Wireless power transfer via strongly coupled magnetic resonances," *Science*, Vol. 317, No. 5834, 83–86, Jul. 2007.

[9] Ahn, D. and S. Hong, "A study on magnetic field repeater in wireless power transfer," *IEEE Transactions on Industrial Electronics*, Vol. 60, No. 1, 360–371, Jan. 2013.

[10] Lu, M. and K. D. T. Ngo, "Attenuation of stray magnetic field in inductive power transfer by controlling phases of windings' currents," *IEEE Transactions on Magnetics*, Vol. 53, No. 9, Sep. 2017.

[11] Lu, M. and K. D. T. Ngo, "Attenuation of stray magnetic field in inductive power transfer by controlling phases of windings' currents," *IEEE Transactions on Magnetics*, Vol. 53, No. 9, Sep. 2017.

[12] Nagai, S., T. Fujita, H. Sumiya, O. Shimizu, and H. Fujimoto, "Reduction of magnetic field by low-order harmonics in magnetic resonant wireless power transfer system using high-frequency switching," *Electrical Engineering in Japan*, Vol. 215, No. 4, Dec. 2022.

[13] Haussmann, N., R. Mease, M. Zang, S. Stroka, H. Hensel, and M. Clemens, "Efficient high-resolution electric and magnetic field simulations inside the human body in the vicinity of wireless power transfer systems with varying models," *Compel-The International Journal For Computation and Mathematics in Electrical and Electronic Engineering*, Vol. 42, No. 4, SI, 903–913, Jun. 2023.

[14] Kim, H., K. Hwang, J. Park, D. Kim, and S. Ahn, "Design of single-sided AC magnetic field generating coil for wireless power transfer," in *2017 IEEE Wireless Power Transfer Conference (WPTC 2017)*, Taipei, Taiwan, May 2017.

[15] Park, S., "Evaluation of electromagnetic exposure during 85 KHz wireless power transfer for electric vehicles," *IEEE*

Transactions on Magnetics, Vol. 54, No. 1, Jan. 2018.

[16] Nguyen, M. Q., Z. Hughes, P. Woods, Y.-S. Seo, S. Rao, and J. C. Chiao, "Field distribution models of spiral coil for misalignment analysis in wireless power transfer systems," *IEEE Transactions on Microwave Theory and Techniques*, Vol. 62, No. 4, 2, SI, 920–930, Apr. 2014.

[17] Guo, Y., J. Li, X. Hou, X. Lv, H. Liang, J. Zhou, and H. Wu, "Poynting vector analysis for wireless power transfer between magnetically coupled coils with different loads," *Scientific Reports*, Vol. 7, Apr. 2017.

[18] Kang, J., Q. Wang, Y. Wang, and W. Li, "Optimization of the magnetic field computation in wireless power transfer system by two-dimensional feature selective validation and maximum value filtered method," *IEEE Transactions on Electromagnetic Compatibility*, Vol. 61, No. 4, 1, 1061–1071, Aug. 2019.

[19] Xianjin, S., L. Guoqiang, Z. Chao, L. Yanhong, and X. Xiaoyu, "Analyses of the coupling model combining field and circuit equations based on solenoidal coils for wireless power transfer," *IET Power Electronics*, Vol. 13, No. 4, 873–880, Mar. 2020.

[20] Chen, Y., K. Chen, S. Zheng, and Z. Zhao, "Analytical model and design method of magnetic core for wireless power transfer magnetic coupler," *Electrical Engineering*, Vol. 23, No. 6, 83–92, Jun. 2022.

[21] Sun, J., "Research on modeling and simulation of wireless charging coupling mechanism based on 3D electromagnetic simulation software," *Electric Machines & Control Application*, Vol. 48, No. 11, 65–71, 2021.